Conformational transition of a non-associative fluorinated amphiphile in aqueous solution

Marc B. Taraban,[1†] Li Yu,[2†] Yue Feng,[1] Elena V. Jouravleva,[3] Mikhail A. Anisimov,[3] Zhong-Xing Jiang,[2] Y. Bruce Yu[1*]

[1]Department of Pharmaceutical Sciences, University of Maryland, Baltimore, MD 21201, USA
[2]School of Pharmaceutical Sciences, Wuhan University, Wuhan, Hubei 430071, China
[3]Department of Chemical and Biomolecular Engineering, University of Maryland, College Park, MD 20742, USA

Table of Contents

Supporting Information

Experimental Section

Synthesis and Characterization

Scheme 1 shows the synthesis FIT-27 (compound **7**), which has 27 chemically equivalent fluorine atoms.

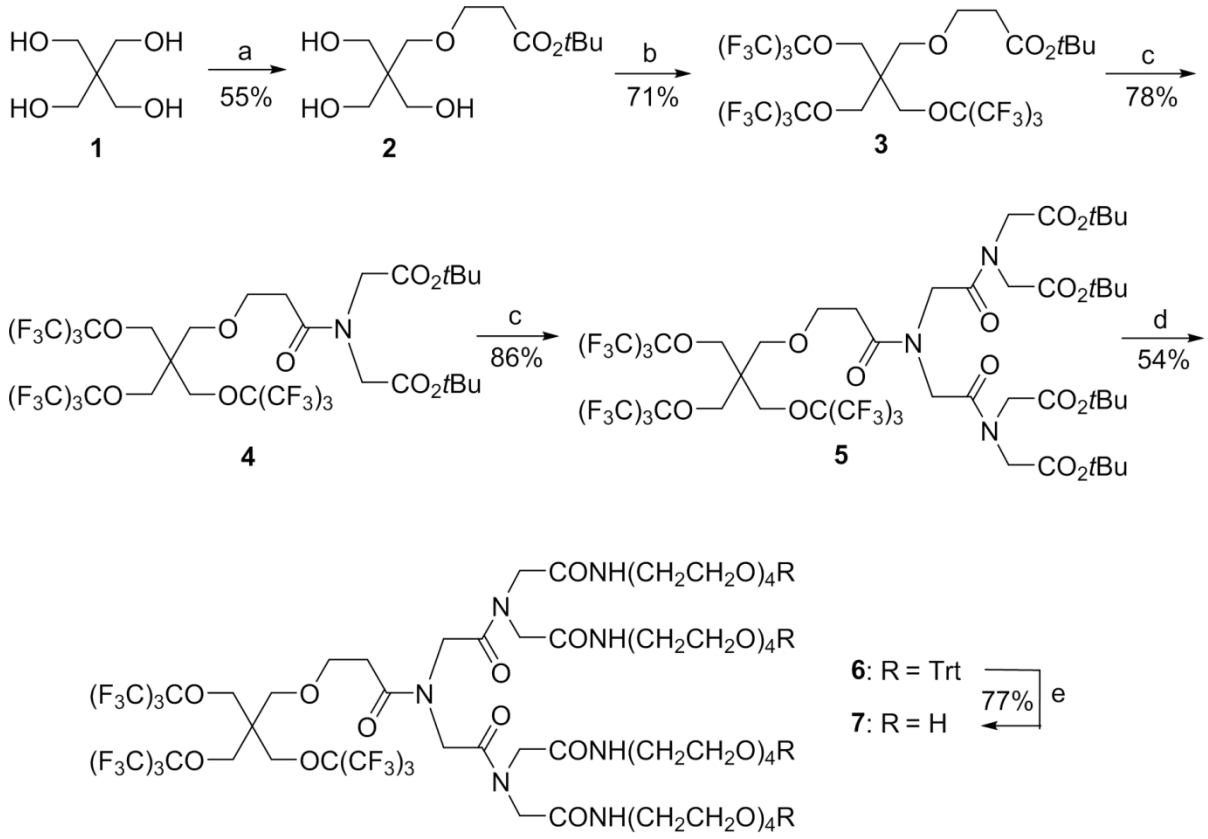

Scheme 1. Synthesis of FIT-27 (7). Reaction conditions: a) *tert*-butyl acrylate, NaOH (aq.), DMSO, 70°C; b) $(CF_3)_3COH$, Ph_3P, DIAD, 4 Å MS, THF; c) (1) TFA, anisole, CH_2Cl_2, rt; (2) DIC, HOBt, DMF/THF (1:1), $HN(CH_2CO_2tBu)_2$, rt; d) (1) TFA, anisole, CH_2Cl_2, rt; (2) DIC, HOBt, DMF/THF (1:1), $H_2N(CH_2CH_2O)_4Trt$, 45°C; e) TosOH, MeOH/THF, rt.

In this version, the *tert*-butyl acrylate was added directly to the pentaerythritol **1** through a Michael addition reaction with a 55% yield to afford triol **2** which then underwent the Mitsunobu reaction with perfluoro-*tert*-butanol to give the fluorinated ester **3** with a 71% yield. With the intermediate **3** at hand,

three cycles of deprotection/condensation were carried out to afford the precursor **6** with high yield. After removal of the trityl protecting group with toluene sulfonic acid, the fluorinated dendrimer **7** was obtained on a 10-g scale. Compared to our previous work,[1] the synthesis procedure here is greatly simplified in two ways. First, 1 of the 4 hydroxyls in compound **1** need to be protected and then deprotected in the older version. In this new version, these two steps were saved by attaching a *tert*-butyl acrylate directly to 1 of the 4 hydroxyls in **1**. This leaves 3 hydroxyls for the Mitsunobu reaction with perfluoro-*tert*-butanol, allowing compound **2** to be conveniently prepared under mild conditions on a 160-g scale. Further, the removal of the *tert*-butyl group in compound **2** is much easier than that of the benzyl group in the older version. As a result, large scale preparation of **7** is made much easier. Second, the trityl group was used to protect 1 of the 2 hydroxyls in tetraethylene glycol. Compared to the benzyl group in the older version for tetraethylene glycol protection, trityl can be introduced and removed much easier and provides much stronger UV signal for reaction monitoring. NMR spectra and MS data of the compounds from Scheme 1 are shown below.

***tert*-Butyl 3-(3-hydroxy-2,2-bis(hydroxymethyl)propoxy)propanoate (2)**. Pentaerythritol **1** (150.2 g, 1.1 mol) and NaOH (8.8 g, 220 mmol, in 20 mL water) were dissolved in DMSO (200 mL) by heating to 70 ^{o}C. Then, *tert*-butyl acrylate (192.2 mL, 1.3 mol) was added drop-wise to the stirred solution for over 2 h at 70 ^{o}C and the resulting mixture was stirred overnight at this temperature. The reaction mixture was cooled to rt, diluted with water (200 mL), and extracted with hexane (100 mL, twice). The aqueous phase was collected. DCM (200 mL, three times) was used to extract the product from the aqueous phase. The combined DCM phase was dried over anhydrous Na_2SO_4, concentrated under vacuum and purified by flash chromatography on silica gel to give **2** as a clear oil (160.5 g, yield 55%). ^{1}H NMR ($CDCl_3$, 400 MHz): δ 1.46 (s, 9H), 2.49 (t, J = 6.0 Hz, 2H), 3.54 (s, 2H), 3.66-3.70 (m, 8H). MS data are presented elsewhere.[2]

***tert*-Butyl 3-(3-((1,1,1,3,3,3-hexafluoro-2-(trifluoromethyl)propan-2-yl)oxy)-2,2-bis(((1,1,1,3,3,3-hexafluoro-2-(trifluoromethyl)propan-2-yl)oxy)methyl)propoxy)propanoate (3)**. To a sealable vessel, alcohol **2** (9.3 g, 35.2 mmol), triphenylphosphine (41.5 g, 158.2 mmol), 4 Å molecular sieves (10.1 g), and dry THF (150 mL) was added under an Ar atmosphere. The resulting mixture was cooled to 0 °C and diisopropyl azodicarboxylate (32.0 g, 158.2 mmol) was added slowly. Afterwards, the mixture was stirred for additional 15 min at rt. Then perfluoro-*tert*-butanol (37.3 g, 158.2 mmol) was added in one portion. The vessel was sealed up and stirred at 45 °C for 48 h. Molecular sieves was

removed by filtration through celite and washed with ether (100 mL). The solution was concentrated and purified by flash chromatography on silica gel to give **3** as white wax (23.0 g, yield 71%). ^{1}H NMR ($CDCl_3$, 400 MHz): δ 1.44 (s, 9H), 2.45 (t, *J* = 8.0 Hz, 2H), 3.42 (s, 2H), 3.64 (t, *J* = 8.0 Hz, 2H), 4.04 (s, 6H); ^{19}F NMR ($CDCl_3$, 376 MHz): δ -73.65. MS data are presented elsewhere.[2]

di-*tert*-Butyl 2,2'-((3-(3-((1,1,1,3,3,3-hexafluoro-2-(trifluoromethyl)propan-2-yl)oxy)-2,2-bis (((1, 1,1,3,3,3-hexafluoro-2-(trifluoromethyl)propan-2-yl)oxy)methyl)propoxy)propanoyl)azanediyl) diacetate 4. To a stirring solution of *tert*-butyl ester **3** (22.3 g, 24.3 mmol) and anisole (3.0 mL, 27.6 mmol) in DCM (100 mL) was added trifluoroacetic acid (29.0 mL). The resulting mixture was stirred at rt for 3 h. Then the reaction mixture was evaporated to dryness under vacuum, and the residue was dissolved in dry DMF/THF (100 mL /100 mL). Then 1-hydroxytriazole (5.0 g, 37.0 mmol) was added. The mixture was cooled to 0 °C and 1,3-diisopropylcarbodiimide (5.8 mL, 4.7 g, 37.0 mmol) was added drop-wise. After stirring for 15 min, di-*tert*-butyl iminodiacetate (7.9 g, 32.3 mmol) was added and the resulting mixture was stirred at rt for 12 h. The solution was washed with brine (150 mL) and extracted with EtOAc (100 mL). The organic phase was collected , dried over anhydrous Na_2SO_4, concentrated under vacuum, and purified by solid-phase extraction on fluorous silica gel to give compound **4** (20.8 g, yield 78%) as clear oil. ^{1}H NMR ($CDCl_3$, 400 MHz) δ 1.46 (s, 9H), 1.47 (s, 9H), 2.54 (t, *J* = 8.0 Hz, 2H), 3.41 (s, 2H), 3.73 (t, *J* = 8.0 Hz, 2H), 3.99 (s, 2H), 4.03 (s, 6H), 4.14 (s, 2H); ^{19}F NMR ($CDCl_3$, 376 MHz) δ -73.63; ^{13}C NMR ($CDCl_3$, 100 MHz) δ 27.4, 27.6, 32.5, 46.0, 48.4, 50.6, 65.5, 66.0, 67.3, 78.9, 79.2, 79.5, 79.8, 81.6, 82.3, 120.0 (q, *J* = 291.0 Hz), 167.8, 168.2, 170.8; MS (MALDI) m/z 1111.8 ($(M+Na)^+$).

***tert*-Butyl 6-(2-(bis(2-(tert-butoxy)-2-oxoethyl)amino)-2-oxoethyl)-3-(2-(tert-butoxy)-2- oxoethyl)-16,16,16-trifluoro-12,12-bis(((1,1,1,3,3,3-hexafluoro-2-(trifluoromethyl)propan-2-yl)oxy)methyl)-4,7-dioxo-15,15-bis(trifluoromethyl)-10,14-dioxa-3,6-diazahexadecan-1-oate 5.** Compound **5** was prepared by following the synthesis of **4** with an 86% yield as a clear oil. ^{1}H NMR ($CDCl_3$, 400 MHz) δ 1.46 (d, *J* = 8.0 Hz, 36H), 2.52 (t, *J* = 8.0 Hz, 2H), 3.41 (s, 2H), 3.70 (t, *J* = 8.0 Hz, 2H), 3.96 (s, 2H), 4.00-4.10 (m, 12H), 4.22-4.30 (m, 4H); ^{19}F NMR ($CDCl_3$, 376 MHz) δ -73.61; ^{13}C NMR ($CDCl_3$, 100 MHz) δ 27.3, 27.46, 27.53, 32.2, 45.8, 45.4, 48.7, 48.9, 49.1, 50.0, 50.4, 65.6, 66.0, 67.4, 78.8, 79.1, 79.4, 79.7, 81.5, 81.6, 82.4, 82.6, 119.9 (q, *J* = 291.0 Hz), 167.4, 167.5, 167.6, 167.7, 169.4, 171.0. MS (MALDI) m/z 1254.7 $(M–2t\text{BuOCO}+Na)^+$. (note: in MS analysis no molecular ion peak of intact **5** was detected.)

Compound 6. To a stirring solution of *tert*-butyl ester **5** (19.1 g, 13.3 mmol) and anisole (3.0 mL, 27.6 mmol) in DCM (100 mL) trifluoroacetic acid (40.0 mL) was added. The resulting mixture was stirred at rt for 3 h. Then the reaction mixture was evaporated to dryness under vacuum, and the residue was dissolved in dry DMF/THF (100 mL /100 mL). 1-Hydroxytriazole (10.8 g, 79.8 mmol) was then added. The mixture was cooled to 0 °C and 1,3-diisopropylcarbodiimide (12.3 mL, 10.1 g, 79.8 mmol) was added drop-wise. After stirring for 5 min, di-*tert*-butyl iminodiacetate (34.7 g, 79.8 mmol) was added and the resulting mixture was stirred at 45 °C for 18 h. The solution was washed with brine (150 mL) and extracted with EtOAc (100 mL). The organic phase was collected , dried over anhydrous Na_2SO_4, concentrated under vacuum, and purified by solid-phase extraction on fluorous silica gel to give compound **6** (20.7 g, yield 54%) as a clear oil. ^{1}H NMR ($CDCl_3$, 400 MHz) δ 2.49 (t, J = 8.0 Hz, 2H), 3.16-3.27 (m, 8H), 3.32-3.42 (m, 10H), 3.45-3.55 (m, 10H), 3.56-3.60 (m, 8H), 3.61-3.78(m, 40H), 3.94(s, 2H), 4.03 (s, 6H), 4.09 (s., 2H), 4.18 (s, 2H), 7.15-7.35 (m, 40H), 7.39-7.52 (m, 24H); ^{19}F NMR ($CDCl_3$, 376 MHz) δ -73.57; ^{13}C NMR ($CDCl_3$, 100 MHz) δ 22.7, 29.4, 29.7, 32.5, 39.3, 46.1, 47.2, 49.4, 52.5, 52.9, 63.4, 65.7, 66.4, 67.5, 69.2, 69.3, 69.4, 70.0, 70.09, 70.14, 70.6, 70.69, 70.74, 86.6, 120.1 (q, J = 291.0 Hz), 127.0, 127.8, 128.7, 144.1, 168.0, 168.4, 168.7, 168.9, 169.2, 170.1, 171.5; MS (MALDI) m/z 2900.3 ($(M+Na)^+$); HRMS (MALDI) calculated for $C_{140}H_{152}N_7O_{27}F_{27}Na^+$, 2899.0217, found, 2899.0197.

Compound 7 (FIT-27). *p*-Toluenesulfonic acid (0.53 g, 2.8 mmol) was added to a solution of **6** (20.0 g, 7.0 mmol) in MeOH/THF (50 mL/50 mL). The mixture was stirred overnight at rt. A solution of NaOH (0.13 g, 3.4 mmol, in 1.5 mL water) was added to the reaction mixture. MeOH was removed under vacuum and the residue was purified by flash chromatography to give compound **7** as a slightly yellowish wax (10.4 g, yield 77%). ^{1}H NMR ($CDCl_3$, 400 MHz) δ 2.58 (t, J = 8.0 Hz, 2H), 3.35-3.50 (m, 10H), 3.52-3.85 (m, 56H), 4.01 (s, 2H), 4.05 (s, 6H), 4.07 (s, 2H), 4.11 (s, 2H), 4.19 (s, 2H), 4.21 (s, 2H), 4.36 (s, 2H); ^{19}F NMR ($CDCl_3$, 376 MHz) δ -73.58; ^{13}C NMR ($CDCl_3$, 100 MHz) δ 21.2, 29.6, 32.4, 39.0, 39.2, 46.0, 47.6, 49.8, 52.0, 52.3, 61.1, 65.6, 66.3, 67.6, 69.2, 69.4, 69.7, 69.9, 70.2, 70.4, 72.4, 79.2, 120.0 (q, J = 291.0 Hz), 125.8, 128.7, 168.4, 168.8, 169.0, 169.2, 169.8, 170.5, 172.0. MS (MALDI) m/z 1931.8 ($(M+Na)^+$); HRMS (MALDI) calcd for $C_{64}H_{96}N_7O_{27}F_{27}Na^+$, 1930.5792, found, 1930.5815.

Sample preparation for physical and structural characterizations

For all characterizations, FIT-27 was dissolved in phosphate-buffered saline (PBS, 50 mM sodium phosphate, 100 mM NaCl, pH 7.4). For all measurements, the solvent was H_2O. The concentration of the stock solution of FIT-27 was 100 mM, and prior to dilutions, the stock solution was filtered through a 0.2-μm filter. To determine the critical concentration, which requires the ^{19}F chemical shift $\delta(^{19}F)$ at different FIT-27 concentrations, solutions in the concentration range of 0.2 to 100 mM were prepared. For all other types of measurements, including PFG NMR, SAXS, SANS and DLS, FIT-27 solutions of 1, 10 and 100 mM were prepared. The solutions of FIT-27 at 1, 10 and 100 mM were respectively well below, slightly above and well above 7.5 mM, the critical concentration of FIT-27 determined by ^{19}F chemical shift measurements.

NMR spectroscopy measurements

All ^1H and ^{19}F NMR experiments were carried out using a Varian INOVA 400 NMR spectrometer (Varian, Inc., 399.75 MHz for ^1H and 376.11 MHz for ^{19}F) equipped with a broadband detection probe with Z-gradient.

200 μL of each FIT-27 solution was placed into a standard 3-mm NMR tube (Norell, Inc.), which was then inserted into a standard 5-mm NMR tube filled with D_2O (deuterium lock) that contains ~ 5mM trifluoroacetic acid (TFA) as the ^{19}F external standard ($\delta_{TFA}(^{19}F)$ = -76.55 ppm[3]). The ^{19}F NMR spectra were collected using the standard one-pulse sequence; for all concentrations, the total number of transients was 64 to attain high S/N ratio.

The self-diffusion coefficient D_s of FIT-27 was measured by the BPP-LED (bipolar pulse longitudinal eddy current delay) method,[4] using the pulsed-field gradient (PFG) NMR technique. Measurement was based on the ^{19}F signal from FIT-27 by monitoring the intensity of the ^{19}F signal as a function of the applied pulsed-field gradient strength, $I(G_z)$, using the following expression:[5]

$$I(G_z) = I_0 \cdot \exp[(-\gamma\delta G_z)^2 \cdot (\Delta - \delta/3) \cdot D_s] \quad (1)$$

wherein γ is the gyromagnetic ratio of the observed nucleus (40.052 MHz/Tesla for ^{19}F of FIT-27 and 42.576 MHz/Tesla for ^1H of H_2O); Δ and δ correspond to the diffusion interval and the length of the PFG pulse respectively; G_z is the gradient strength and I_0 is the initial intensity of the signal. D_s of H_2O in the same samples was measured as a reference point. The diffusion interval time Δ was 400 ms for FIT-27 in ^{19}F measurements and 200 ms for H_2O in ^1H measurements. The length of PFG pulse δ was 8

ms for FIT-27 in ^{19}F measurements and 4 ms for H_2O in ^{1}H measurements. For both ^{19}F and ^{1}H measurements, the pulsed-field gradient strength G_z increased linearly from 0.9 Gs/cm to 13.6 Gs/cm to gain sufficient signal decay in 16 steps .

Small-Angle X-Ray Scattering (SAXS) and Small-Angle Neutron Scattering (SANS)

In SAXS experiments, 25 μL of each solution were pumped into a cylindrical quartz capillary cell using the autosampler of the instrument (BioSAXS-1000, Rigaku Co.). For SANS experiments, 400 μL of each solution were aliquoted into a titanium cell with 1-mm path length between two quartz windows each of 30-mm in diameter, which is routinely used for SANS measurements at the National Institute of Standards and Technology (NIST) Center for Neutron Research (NCNR).

Solution X-ray scattering data were acquired on the BioSAXS-1000 (Rigaku Co.) instrument equipped with confocal Max-Flux optics. Data collection was done using the Pilatus 100K (Dectris, Ltd.) detector positioned 0.48 m from the sample capillary with 8 keV Cu Kα incident radiation from the Micromax-007HF rotating anode source resulting in the observable Q-range of ~ 0.009–0.70 $Å^{-1}$. Scattered radiation was detected, subject to a 7-keV low-energy cutoff. Q-axis mapping was done using scattering from a silver behenate standard sample. A total of 16 sequential data frames with exposure time of 30 min were recorded with the samples kept at 25°C throughout the measurement. Individual data frames were checked for evidence of radiation damage. The composite 8 h images were then masked, corrected for detector sensitivity, radially integrated, and normalized by the corresponding transmitted beam intensities. Buffer scattering was subtracted from sample scattering.

$I(Q)$ is the scattering intensity of X-rays, and Q is the scattering vector amplitude which is related to the X-ray wavelength λ and the scattering angle 2θ by

$$Q = \frac{4\pi}{\lambda}\sin\theta \qquad (2)$$

SANS data were collected using a 30-m SANS instrument (NG-3) at NIST.[6] Monochromatic neutrons at λ = 6 Å with a wavelength spread ($\Delta\lambda/\lambda$) of 0.14 were detected on a 64 cm × 64 cm two-dimensional detector. Data on SANS intensity were collected with a Q-range from 0.001 $Å^{-1}$ to 0.4 $Å^{-1}$. The low-Q configuration used neutron focusing lenses and an 8 Å neutron wavelength. Scattering

intensities were normalized using direct beam transmission measurements and were reduced according to published protocols.[7] Both SAXS and SANS instruments have pinhole geometry.

The solution structures of FIT-27 were studied at 1 mM and 10 mM concentrations in SAXS experiments and at 10 mM concentration in SANS experiments, and the data were processed using the ATSAS software.[8,9] Unfortunately, SANS data at 1 mM FIT-27 in H_2O show very weak signal, and could not be processed reliably. Scattering data (both SAXS and SANS) at high concentration (at 100 mM) show strong structure factor peak, and, therefore, cannot be analyzed using the approaches applied to dilute solutions. However, these data could be used for the analysis of size distribution and structure factor (see below).

The analysis of pair-wise distance distribution functions for globular particles $P(r)$ (Eq. 3) was performed using the linear regularization method of indirect Fourier-transformation using the program GNOM.[8]

$$P(r) = \frac{1}{2\pi^2}\int I(Q)\cdot(Q\cdot r)\cdot\sin(Q\cdot r)dQ \qquad (3)$$

$P(r)$ is proportional to the probability of finding different vector lengths connecting two unit-volume elements within the scattering particle, and $P(r) = 0$ happens at the maximum linear dimension of the scattering particle, d_{max} (i.e., for $r \geq d_{max}$, $P(r) = 0$). The radius of gyration of the scattering globular particle, R_g, is derived from the second moment of $P(r)$ as:

$$R_g^2 = \frac{\int_0^{d_{max}} P(r)r^2dr}{2\int_0^{d_{max}} P(r)dr} \qquad (4)$$

R_g is the root mean square distance of all unit-volume elements from the center of gravity of the scattering particle weighted by the scattering contrasts, and in the case of X-rays, the distribution of the mass is defined by the electron density distribution within the scattering particle. A simulated annealing algorithm was used to restore low resolution 3D structures of FIT-27 in 1 mM and 10 mM solutions built from densely packed dummy atoms implemented in the DAMMIF program.[10] To build the most

probable and reliable 3D model, multiple DAMMIF solutions (at least 25 runs for each 1 mM and 10 mM FIT-27 solutions) were aligned using the best matching alignment program SUPCOMB[11] and averaged using the DAMAVER routine.[12] The normalized structural discrepancy parameter (NSD), which characterizes structural similarity of DAMMIN results, was ~0.4 for both substances (NSD = 0 for ideal similarity, and NSD > 1 for systemically different structures).

IRENA 2.46 software[13] for *IGOR Pro 6.3* (WaveMetrics, Inc.) was used to analyze the size distribution and structure factor in 100 mM FIT-27 solution.

The analysis employs basic representation of the scattering profile:[13]

$$I(Q) \sim \int_0^\infty \left|P(Q,r)\right|^2 \cdot V^2(r) \cdot N \cdot \Pi(r) \cdot dr \qquad (5)$$

where $P(Q, r)$ is the form factor of the scattering particle, $V(r)$ is the particle volume, N is the total number of scattering particles, and $\Pi(r)$ is the probability to find the scattering particle with size r. Spheroid form factor with fitted aspect ratio (within the limits from 0.3 to 1.0, in order to allow for oblate shape) was used for the form factor modeling. Structure factor analysis was based on the approach suggested for hard spheres[7] which demonstrated the best conformity to our experimental data.

Dynamic Light Scattering (DLS) Experiments

Prior to DLS experiments, all samples were additionally filtered through a 0.2 μm filter. One mL of each sample was aliquoted into cylindrical glass vials (6 mm in diameter). Data collection started after complete equilibration at 25 °C (± 0.1 °C) in the cavity of the light scattering setup. The scattering angle in all experiments was 90°.

DLS experiments were performed with a PhotoCor Instruments equipment,[14] and the software *DynaLS* (SoftScientific, Inc.) was used to process the scattering data. For a single-exponentially decaying relaxation process, the intensity autocorrelation function $g_2(t)$ (obtained in the homodyning mode) is given as[15]

$$g_2(t) - 1 = A \exp[-2\frac{t}{\tau}] \qquad (6)$$

where A is the amplitude of the relaxation process, t is the "lag" (or "delay") time of photon correlations, and τ is the characteristic relaxation time of the polarization fluctuations which essentially give rise to light scattering. For a diffusive relaxation process, the decay (relaxation) time τ reflects the average time of the particle travels within the laser spot of the instrument and, thus, is related to particle mobility, and, hence, the collective diffusion coefficient D_c as[34]

$$\tau = \frac{1}{D_c q^2} \tag{7}$$

where q is the difference in the wave vectors between the incident and scattered light,

$$q = \frac{4\pi n \sin(\frac{\theta}{2})}{\lambda} \tag{8}$$

n is the refractive index of the solvent (1.33245095 for water), λ is the wavelength of the incident light in vacuum (λ = 633 nm for a He−Ne laser), and θ is the scattering angle (90°). Hence, in our experiments, q = 0.0187 nm^{-1}. For monodisperse, non-interacting, spherical Brownian particles, the hydrodynamic radius R_h can be calculated with the Stokes-Einstein relation[34]

$$R_h = \frac{k_B T}{6\pi\eta D_c} \tag{9}$$

where k_B is Boltzmann's constant (1.381×10^{-23} J/K), T is the absolute temperature (298 Kelvin), and η is the viscosity of the solvent ($8.93904021 \times 10^{-4}$ Pa·s for water at 25°C).

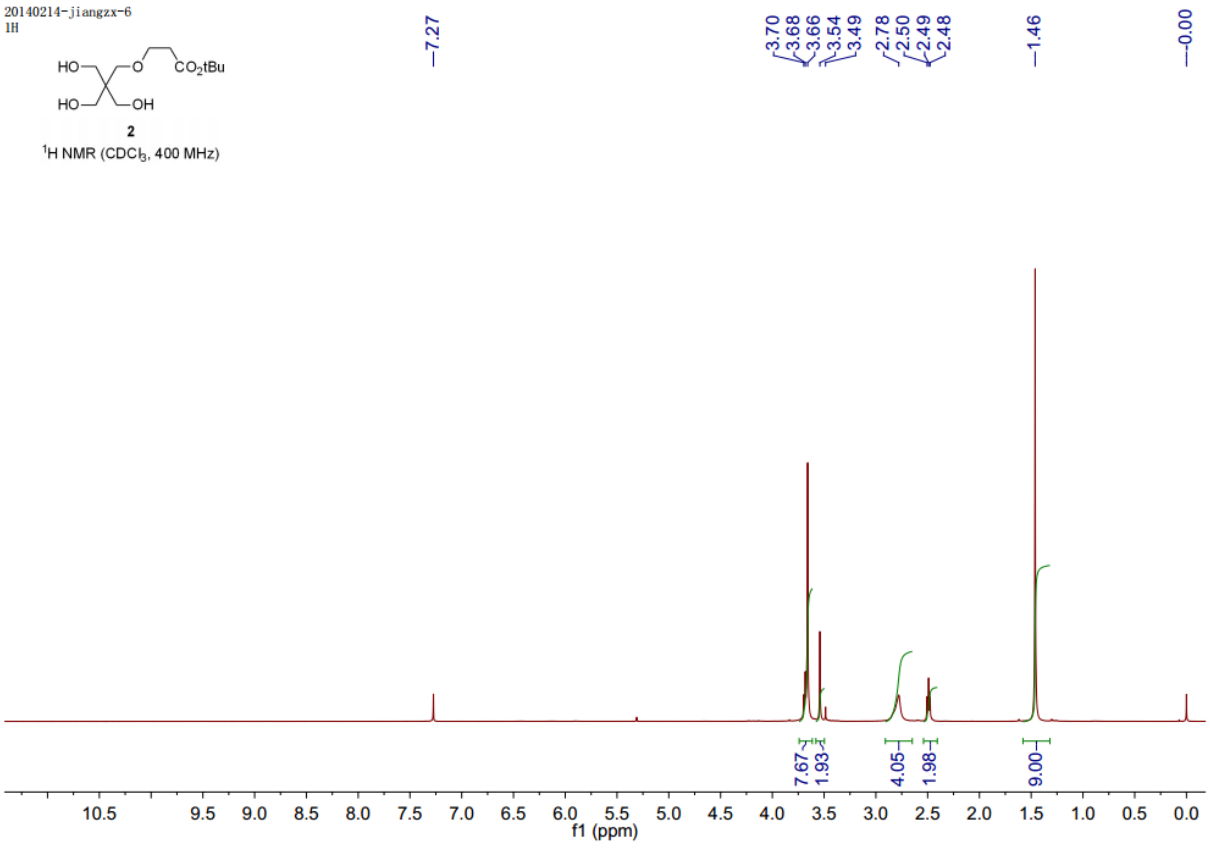

Figure S1. ^{1}H NMR spectrum of compound **2** in $CDCl_3$ (see, Scheme 1).

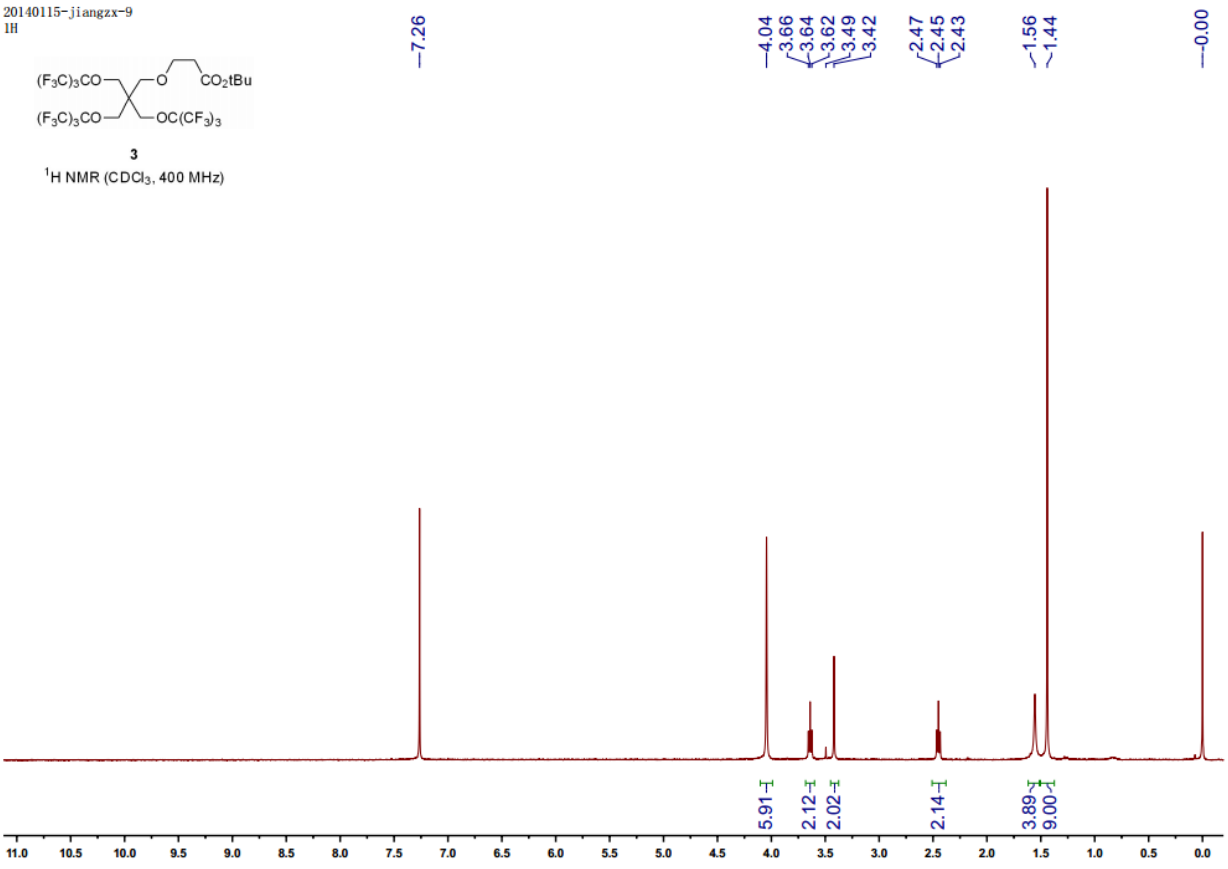

Figure S2. ^{1}H NMR spectrum of compound **3** in $CDCl_3$ (see, Scheme 1).

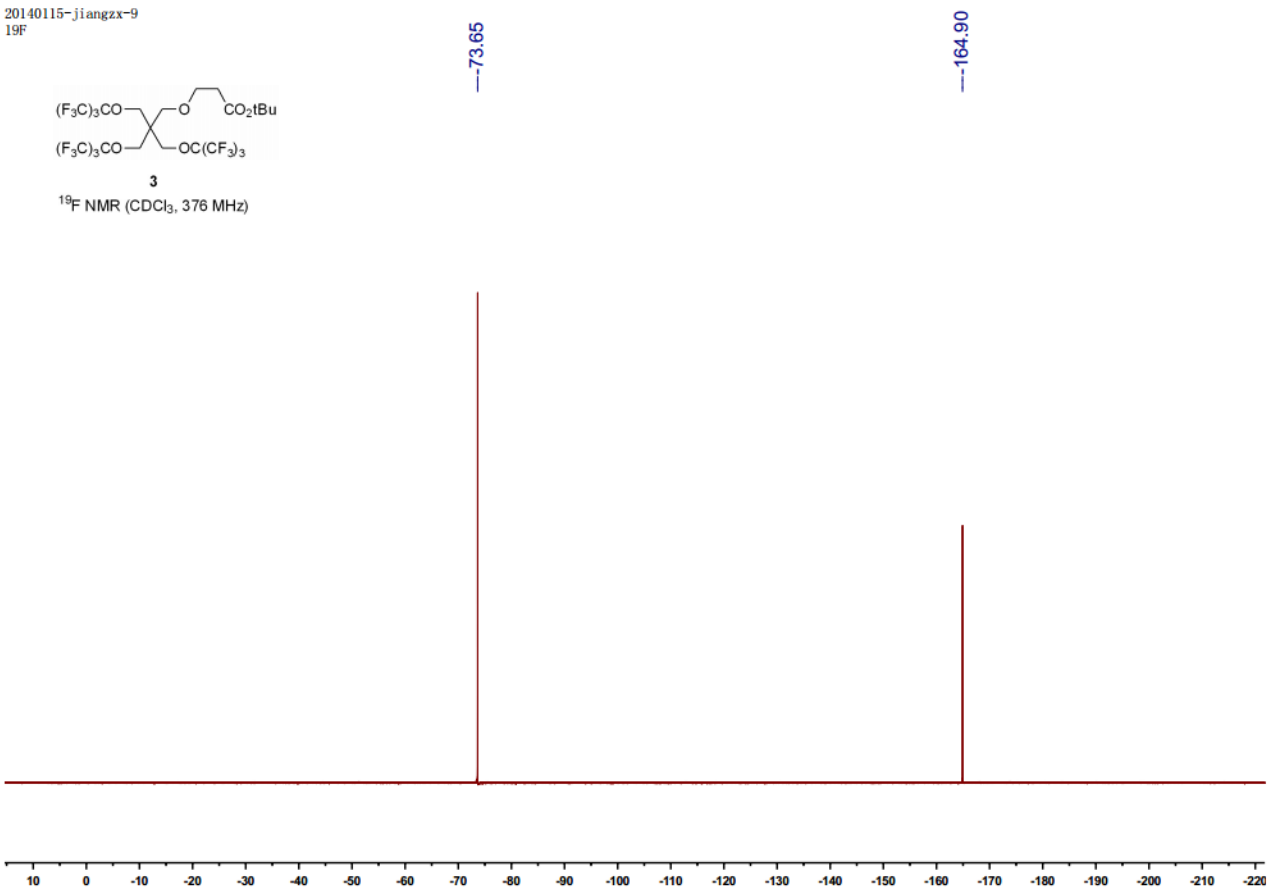

Figure S3. ^{19}F NMR spectrum of compound **3** in $CDCl_3$ (see, Scheme 1).

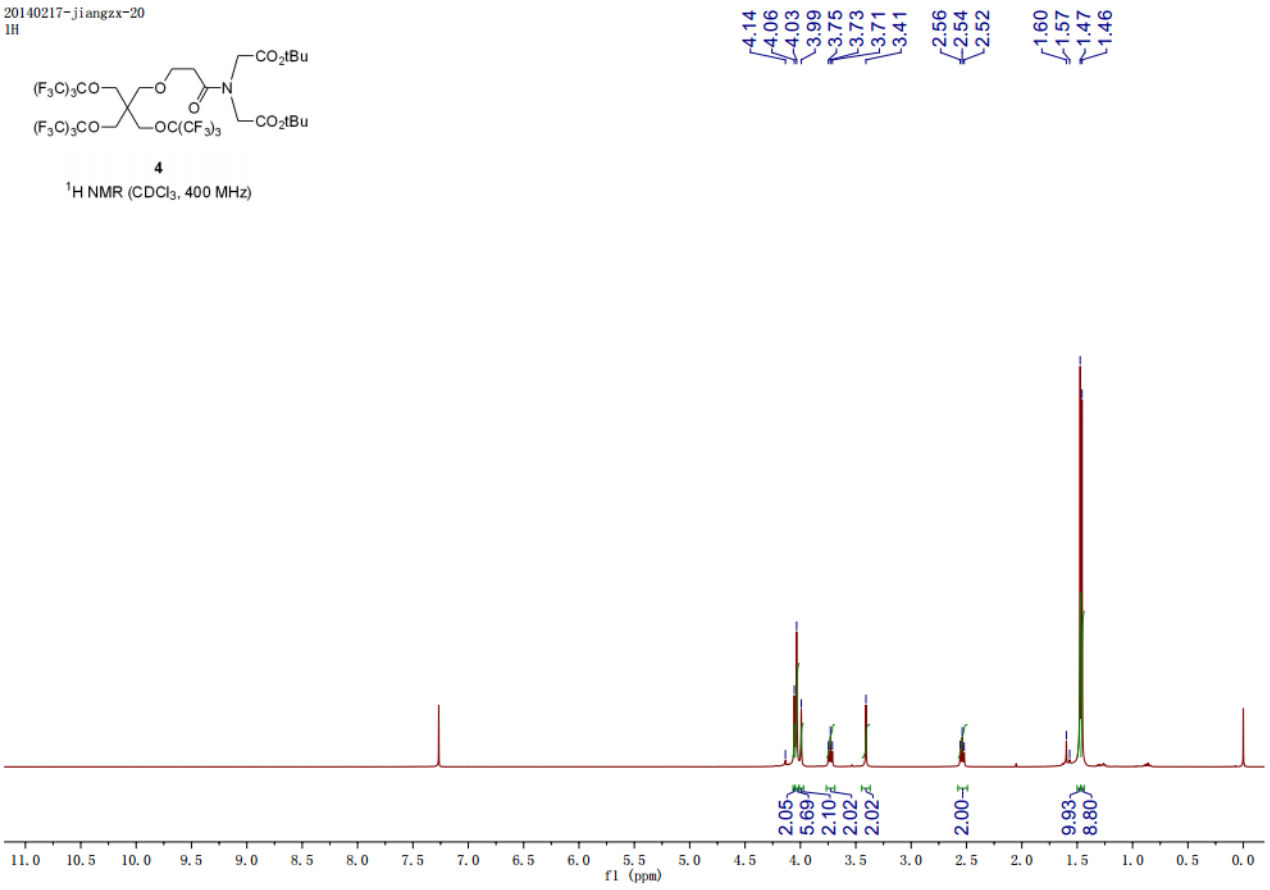

Figure S4. ^{1}H NMR spectrum of compound **4** in $CDCl_3$ (see, Scheme 1).

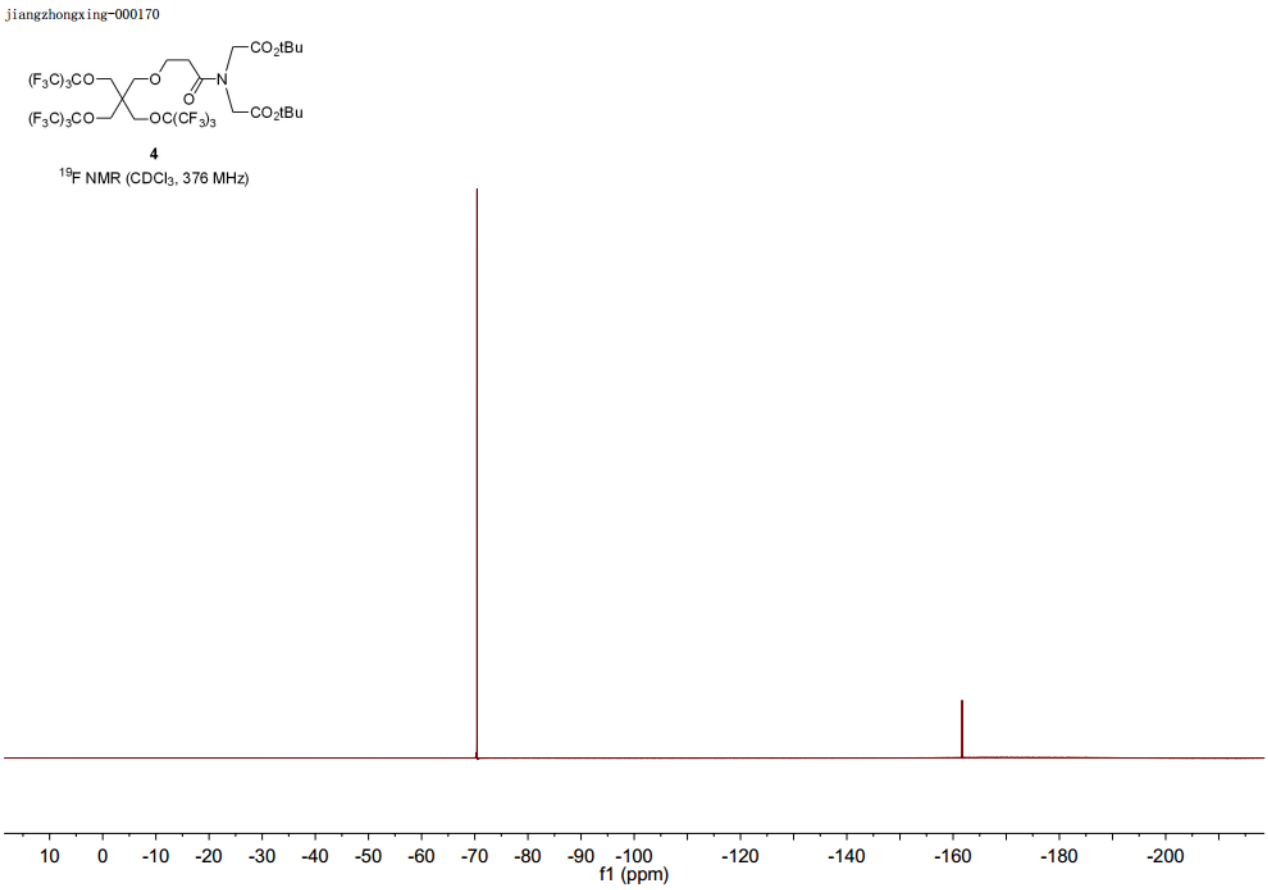

Figure S5. ^{19}F NMR spectrum of compound **4** in $CDCl_3$ (see, Scheme 1).

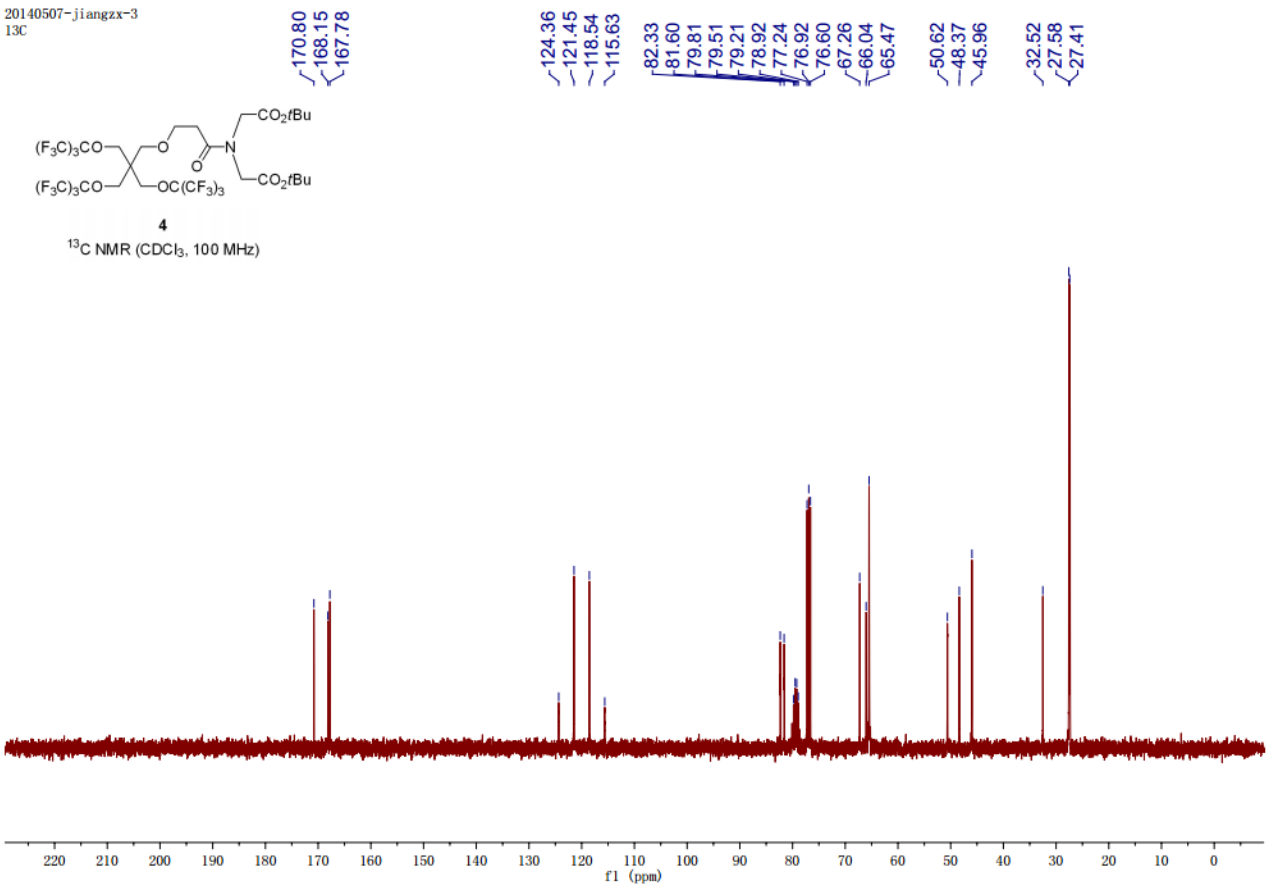

Figure S6. ^{13}C NMR spectrum of compound **4** in $CDCl_3$ (see, Scheme 1).

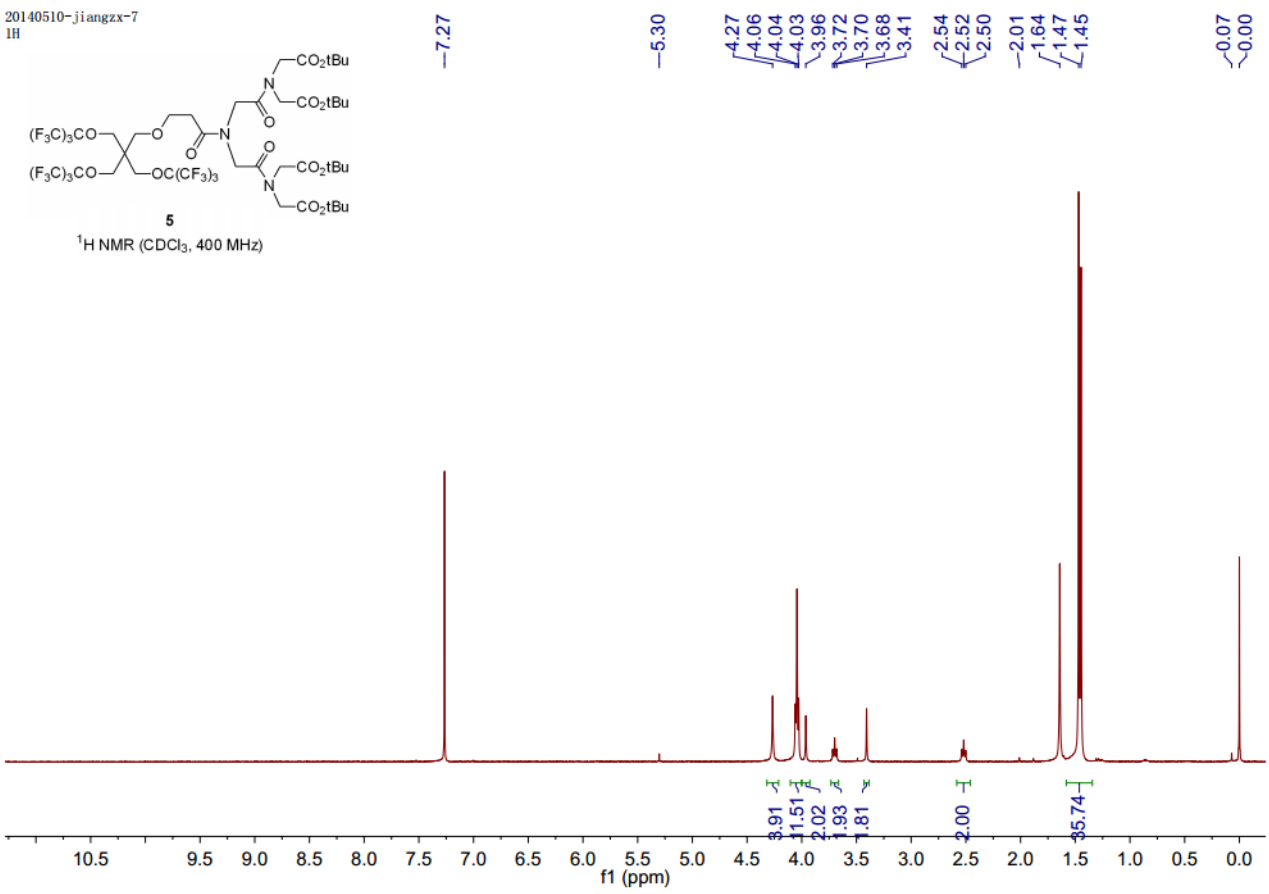

Figure S7. ^{1}H NMR spectrum of compound **5** in $CDCl_3$ (see, Scheme 1).

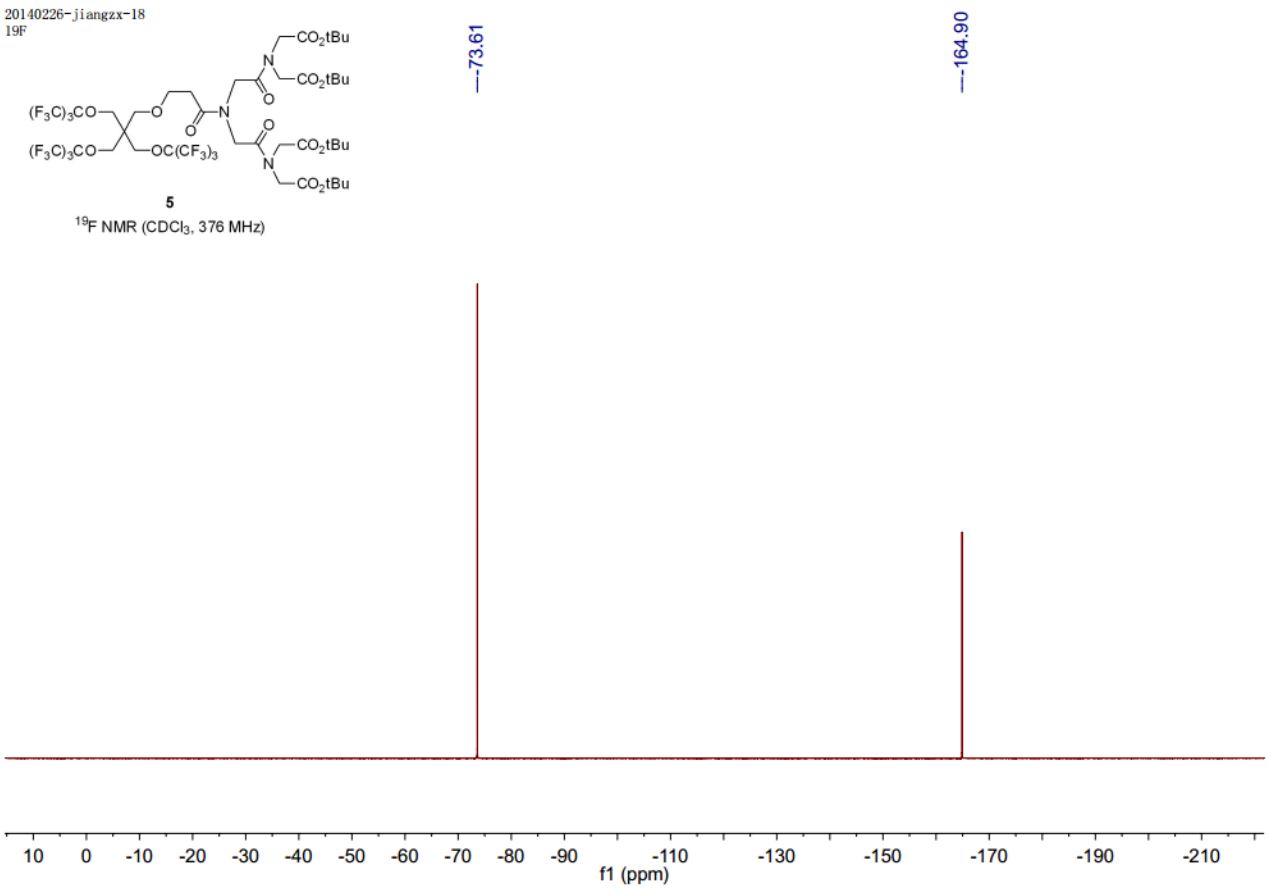

Figure S8. ^{19}F NMR spectrum of compound **5** in $CDCl_3$ (see, Scheme 1).

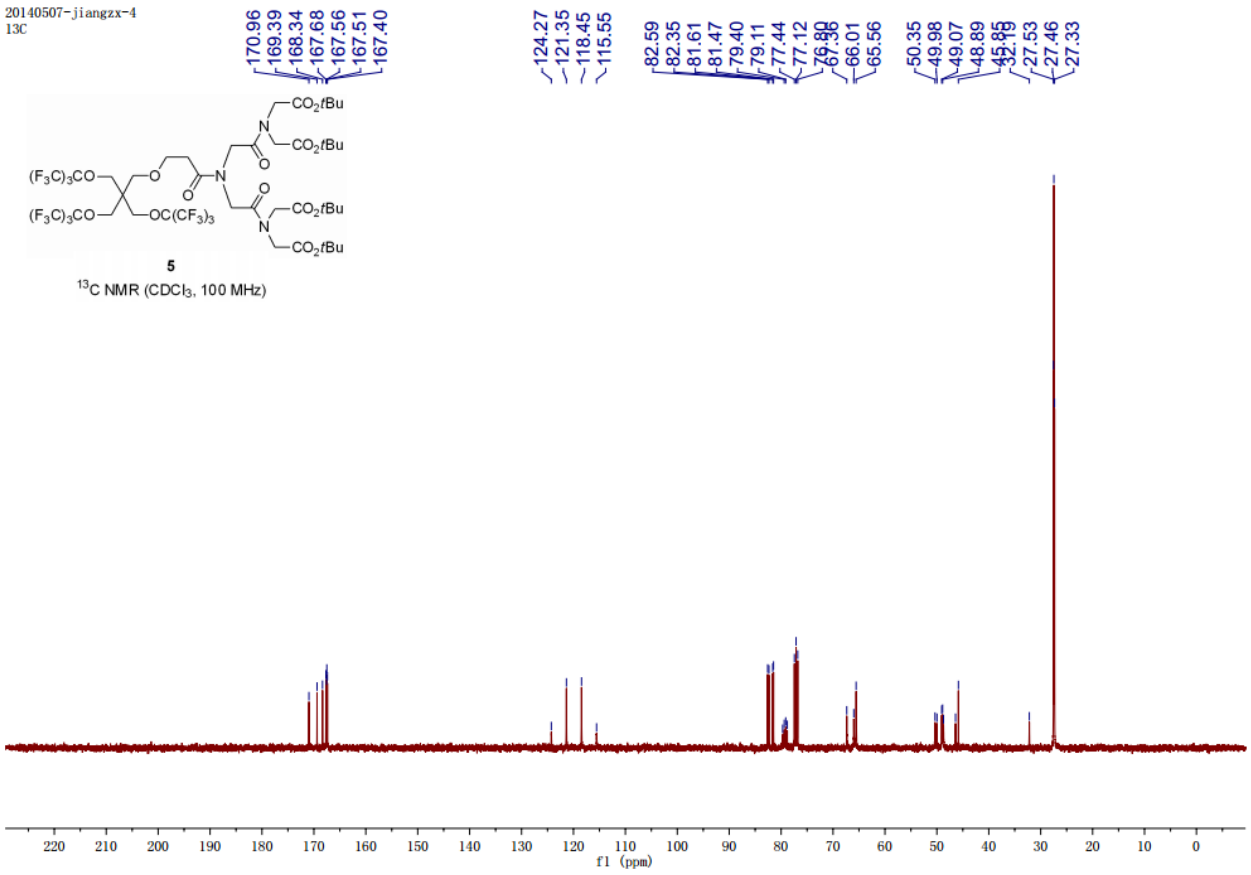

Figure S9. ^{13}C NMR spectrum of compound **5** in $CDCl_3$ (see, Scheme 1).

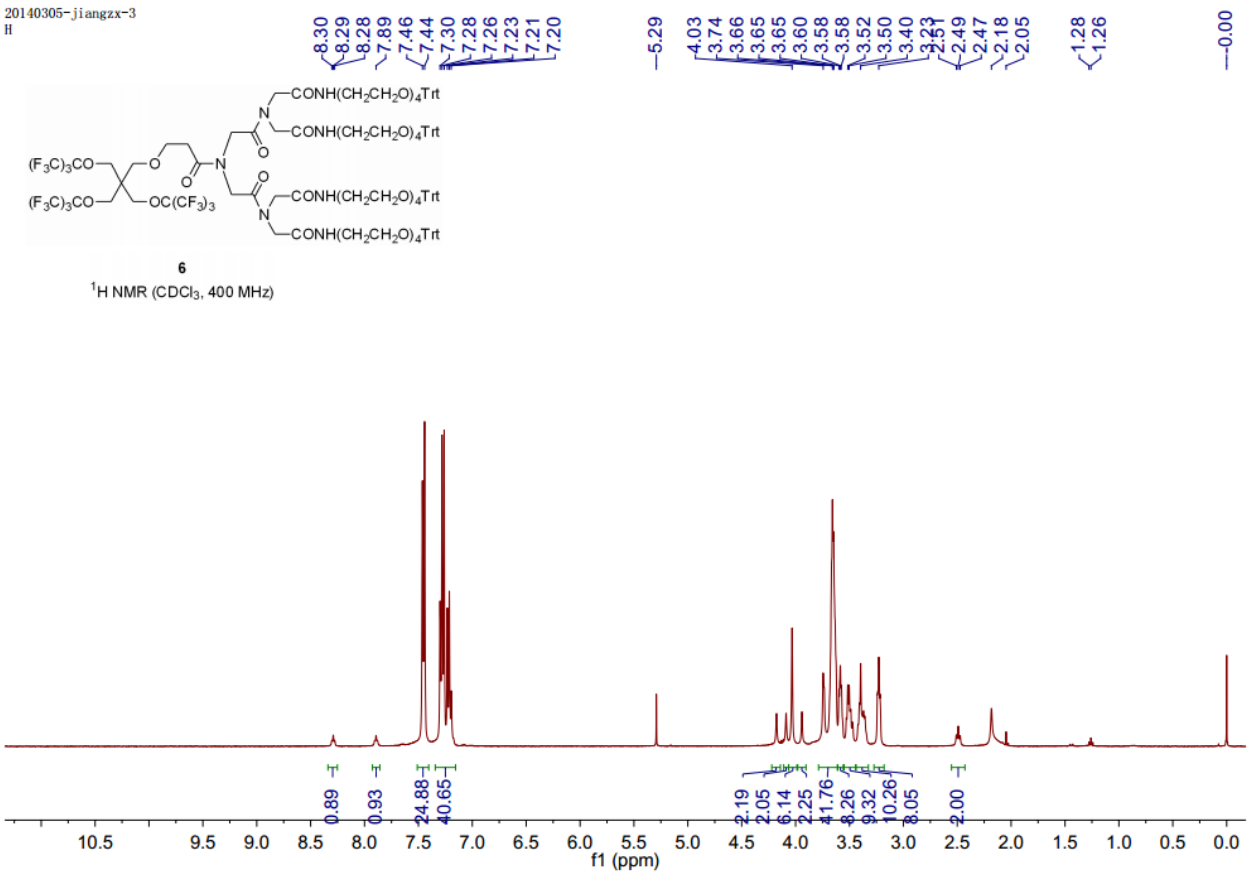

Figure S10. ^{1}H NMR spectrum of compound **6** in $CDCl_3$ (see, Scheme 1).

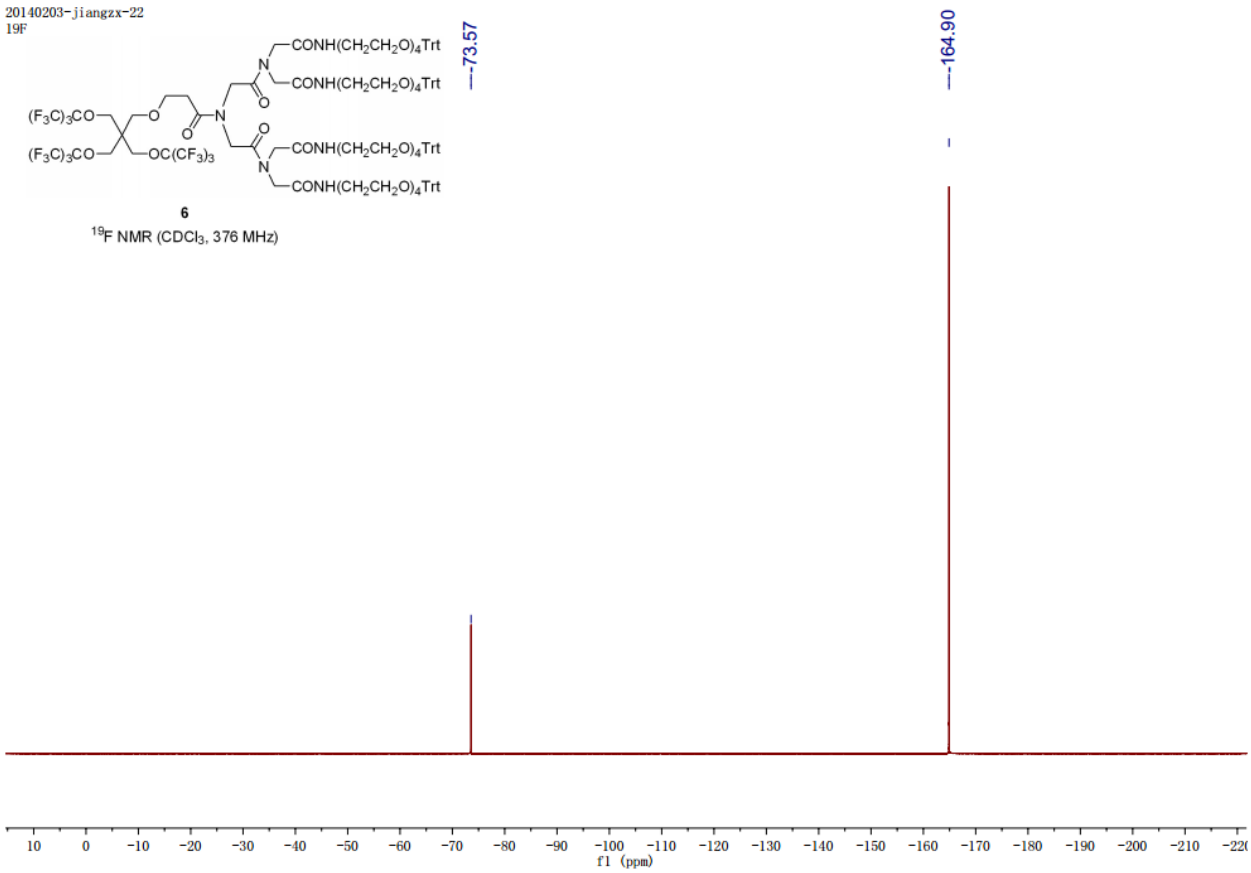

Figure S11. ^{19}F NMR spectrum of compound **6** in $CDCl_3$ (see, Scheme 1).

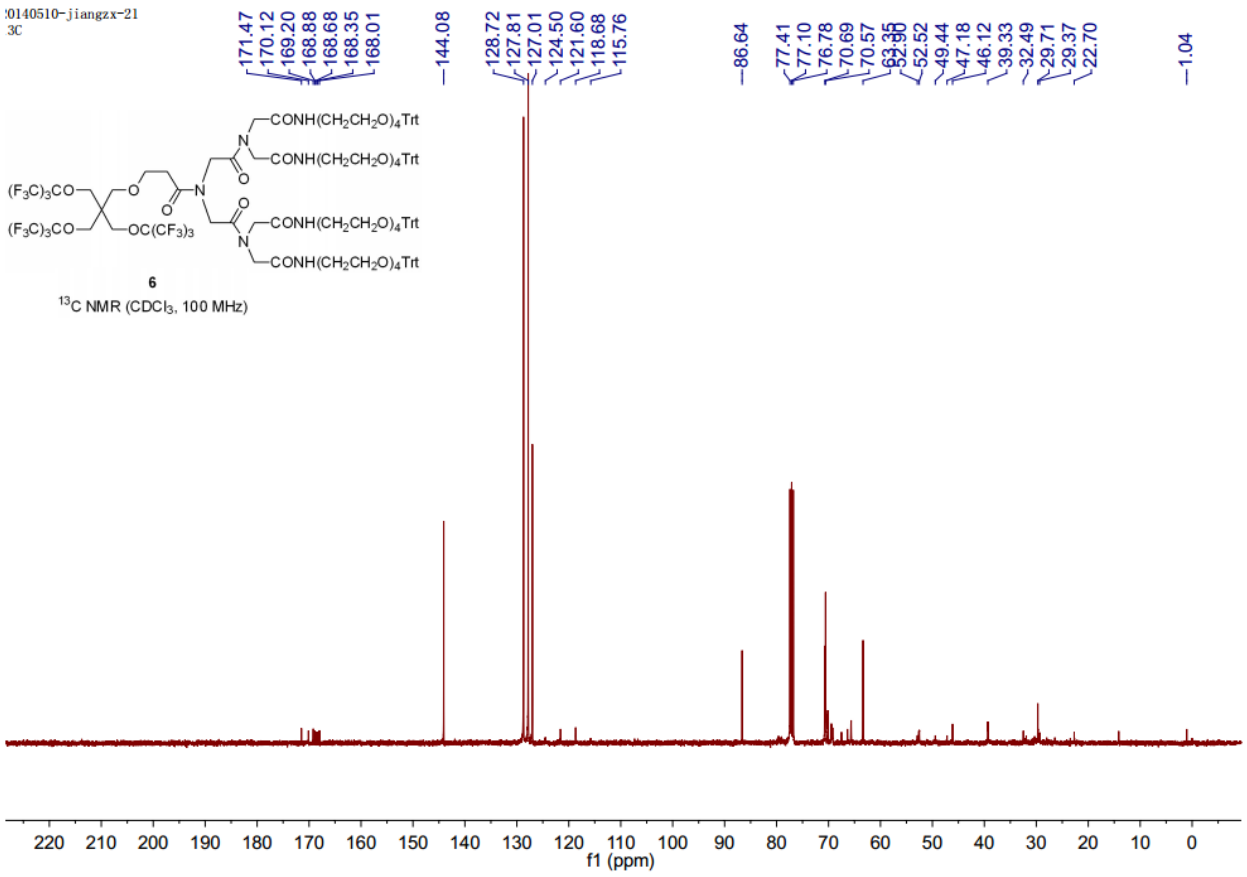

Figure S12. ^{13}C NMR spectrum of compound **6** in $CDCl_3$ (see, Scheme 1).

Shanghai Mass Spectrometry Center
Shanghai Institute of Organic Chemistr
Chinese Academic of Sciences
High Resolution MS DATA REPORT

Instrument: IonSpec 4.7 Tesla FTMS

Card Serial Number : I14 855

Sample Serial Number: FIT-026

Operator : HuaQin Date: 2014/05/16

Operation Mode: MALDI/DHB

Elemental Composition Search Report:

Target Mass:

Target m/z = 2899.0217 ± 0.005
Charge = +1

Possible Elements:

Element:	Exact Mass:	Min:	Max:
C	12.000000	0	140
H	1.007825	0	160
N	14.003074	5	9
O	15.994915	25	29
F	18.998403	25	29
Na	22.989770	1	1

Additional Search Restrictions:

DBE Limit Mode = Both Integer and Half-Integer
Minimum DBE = 0

Search Results:

Number of Hits = 6

m/z	Delta m/z	DBE	Formula
2899.02201	-0.00031	61.5	$C_{134}H_{154}N_7O_{29}F_{29}Na^{+1}$
2899.02087	0.00083	65.0	$C_{137}H_{153}N_7O_{28}F_{28}Na^{+1}$
2899.02355	-0.00185	69.5	$C_{140}H_{151}N_8O_{25}F_{28}Na^{+1}$
2899.01973	0.00197	68.5	$C_{140}H_{152}N_7O_{27}F_{27}Na^{+1}$
2899.02469	-0.00299	66.0	$C_{137}H_{152}N_8O_{26}F_{29}Na^{+1}$
2899.02603	-0.00433	65.5	$C_{139}H_{154}N_5O_{27}F_{29}Na^{+1}$

Figure S13. MALDI results for compound **6** (see, Scheme 1).

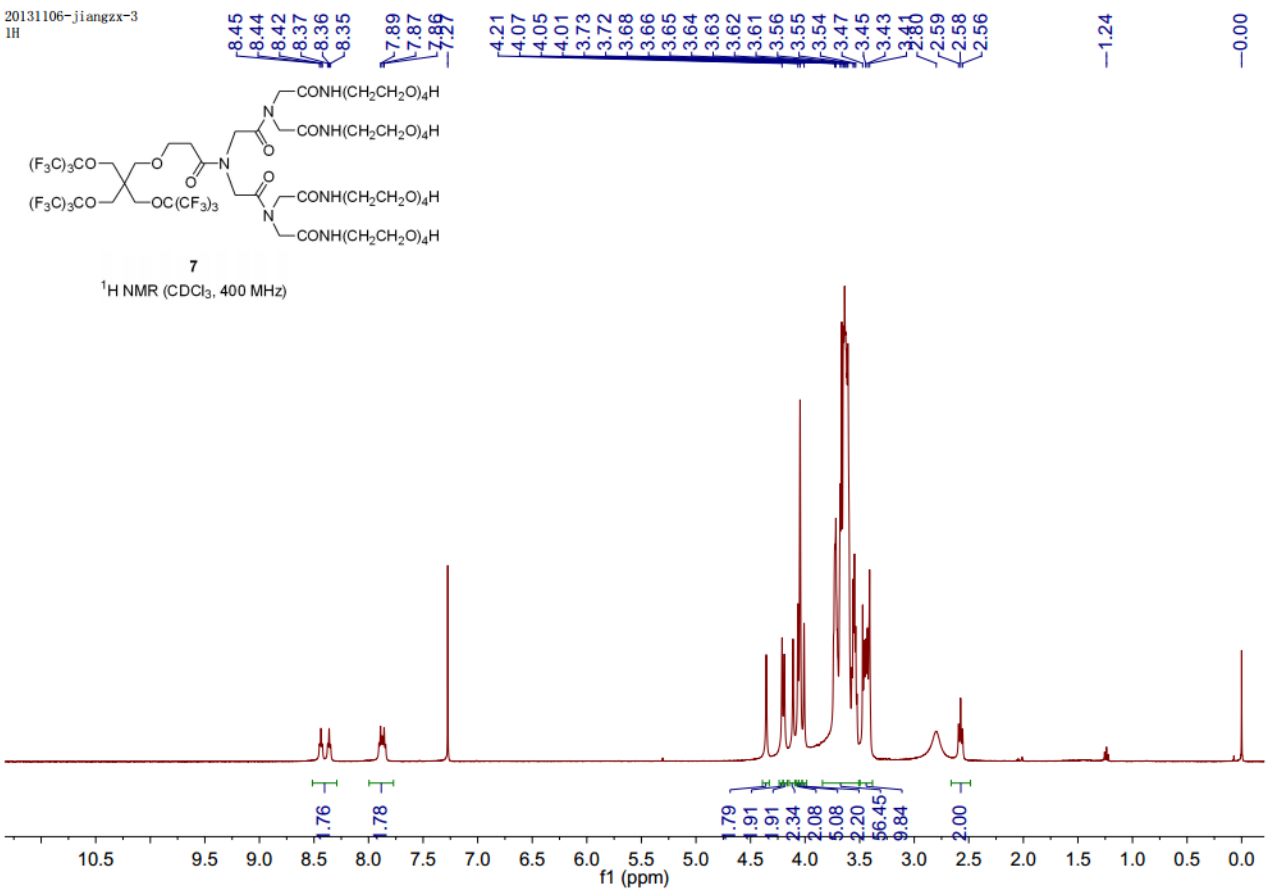

Figure S14. ^{1}H NMR spectrum of compound **7** (FIT-27) in $CDCl_3$ (see, Scheme 1).

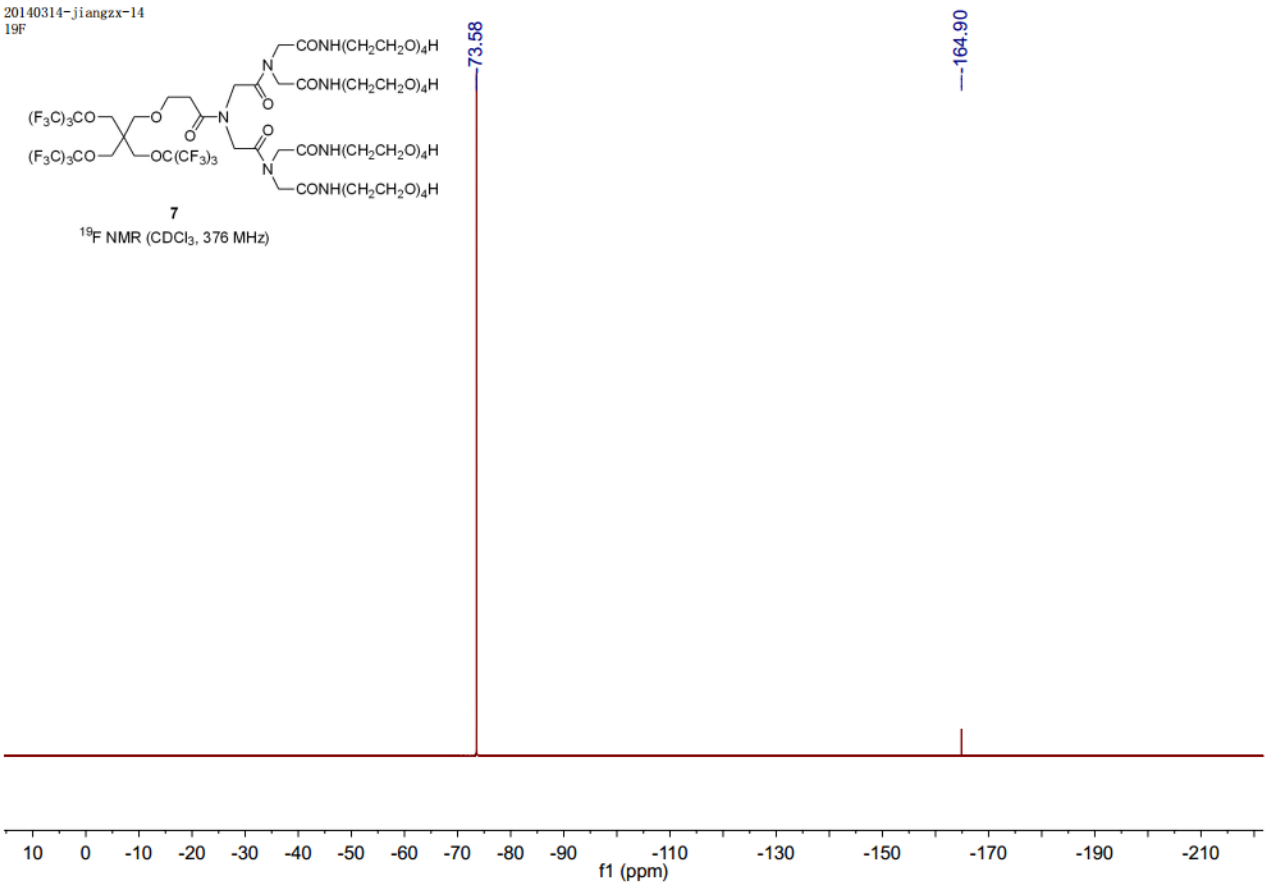

Figure S15. ^{19}F NMR spectrum of compound **7** (FIT-27) in $CDCl_3$ (see, Scheme 1).

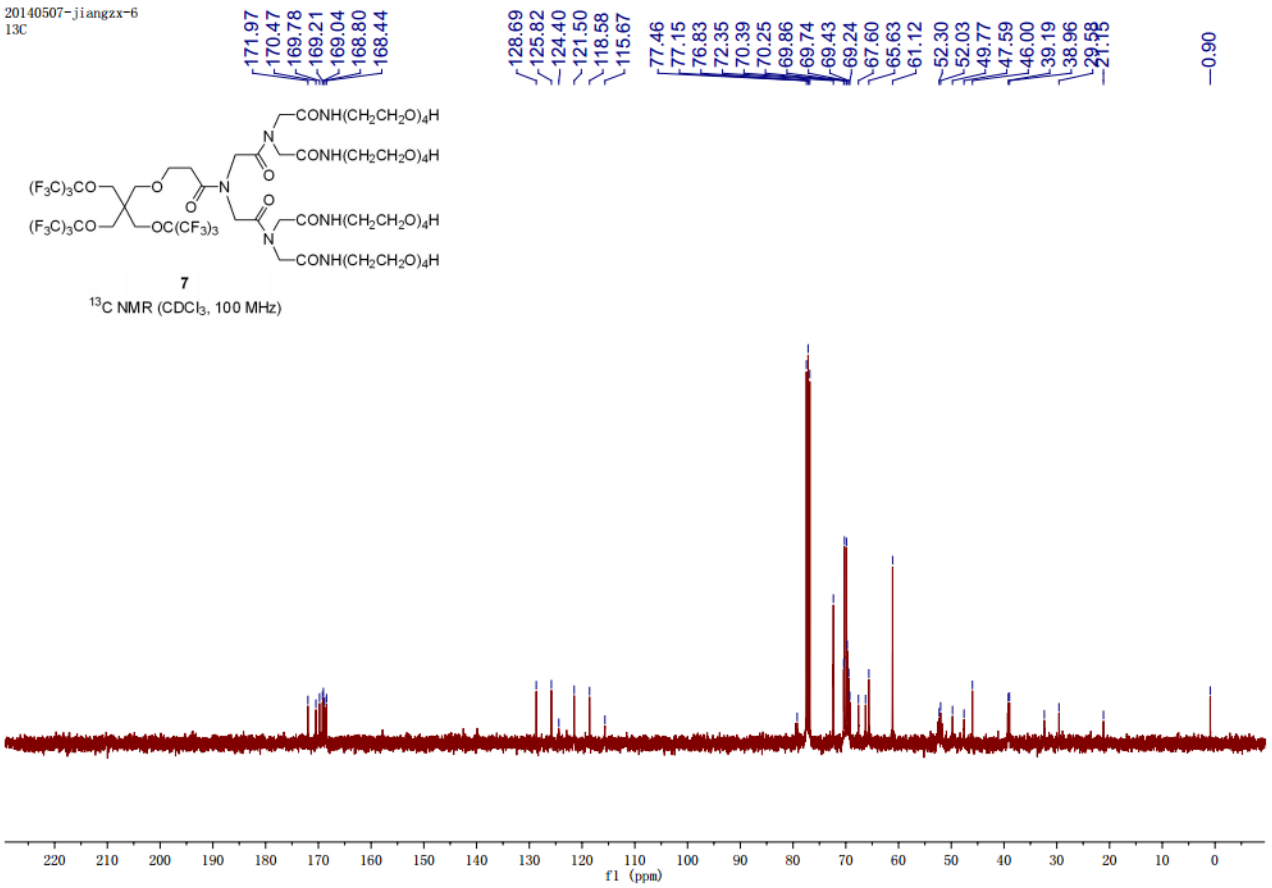

Figure S16. ^{13}C NMR spectrum of compound **7** (FIT-27) in $CDCl_3$ (see, Scheme 1).

Shanghai Mass Spectrometry Center
Shanghai Institute of Organic Chemistr
Chinese Academic of Sciences
High Resolution MS DATA REPORT

Instrument: IonSpec 4.7 Tesla FTMS

Card Serial Number : I14 856

Sample Serial Number: FIT-027

Operator : HuaQin Date: 2014/05/16

Operation Mode: MALDI/DHB

Elemental Composition Search Report:

Target Mass:
Target m/z = 1930.5792 ± 0.005
Charge = +1

Possible Elements:

Element:	Exact Mass:	Min:	Max:
C	12.000000	0	100
H	1.007825	0	100
N	14.003074	5	9
O	15.994915	25	29
F	18.998403	25	29
Na	22.989770	1	1

Additional Search Restrictions:
DBE Limit Mode = Both Integer and Half-Integer
Minimum DBE = 0

Search Results:
Number of Hits = 11

m/z	Delta m/z	DBE	Formula
1930.57924	-0.00004	27.5	$C_{70}H_{94}N_7O_{25}F_{25}Na^{+1}$
1930.58038	-0.00118	24.0	$C_{67}H_{95}N_7O_{26}F_{26}Na^{+1}$
1930.57770	0.00150	19.5	$C_{64}H_{97}N_6O_{29}F_{26}Na^{+1}$
1930.57750	0.00170	16.5	$C_{59}H_{96}N_9O_{29}F_{27}Na^{+1}$
1930.58153	-0.00233	20.5	$C_{64}H_{96}N_7O_{27}F_{27}Na^{+1}$
1930.57656	0.00264	23.0	$C_{67}H_{96}N_6O_{28}F_{25}Na^{+1}$
1930.57636	0.00284	20.0	$C_{62}H_{95}N_9O_{28}F_{26}Na^{+1}$
1930.58267	-0.00347	17.0	$C_{61}H_{97}N_7O_{28}F_{28}Na^{+1}$
1930.57526	0.00394	18.0	$C_{62}H_{96}N_6O_{27}F_{29}Na^{+1}$
1930.57522	0.00398	23.5	$C_{65}H_{94}N_9O_{27}F_{25}Na^{+1}$
1930.58381	-0.00461	13.5	$C_{58}H_{98}N_7O_{29}F_{29}Na^{+1}$

Figure S17. MALDI results for **compound 7 (FIT-27)** (see, Scheme 1).

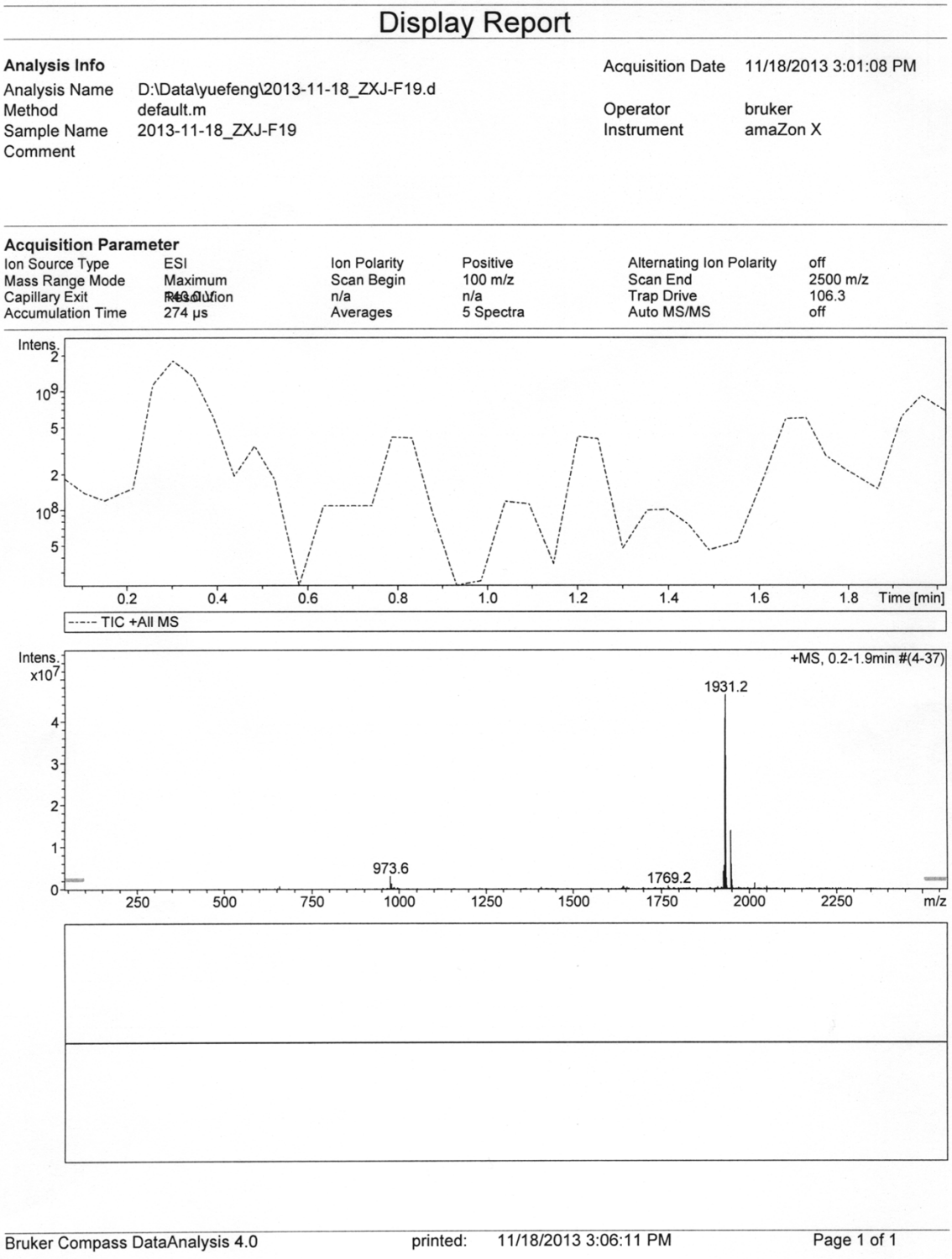

Figure S18. ESI MS results for compound **7** (FIT-27)

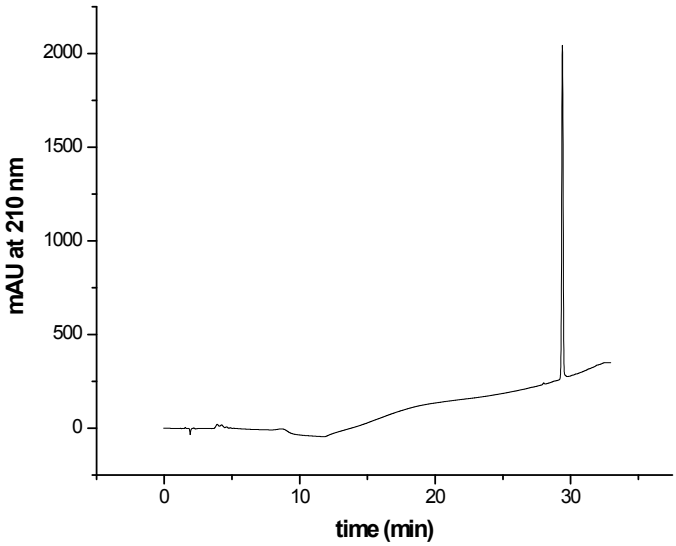

Figure S19. Analytical HPLC chromatogram for compound **7** (FIT-27). Trace amount sample was dissolved in water. HPLC column: Eclipse XDB C-18, 5 μm, 4.6 × 150 mm. eluent A: 0.1 % TFA in water; eluent B: 0.1 % TFA in methanol. Gradient method: 0-100 % B in 30 min. rt.

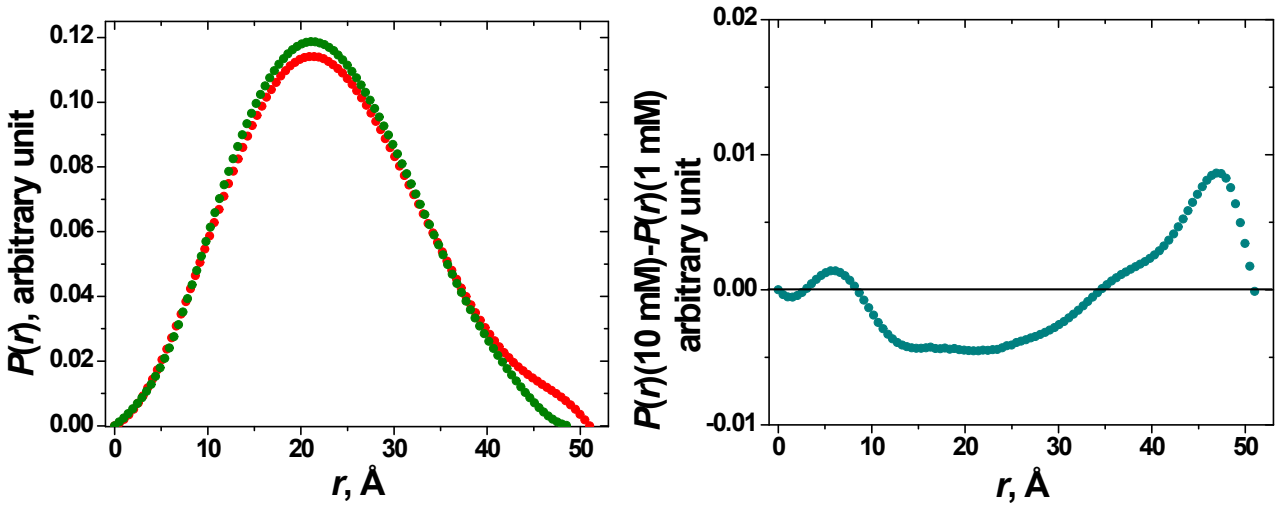

Figure S20. (Left) Comparison of pair-wise distance distribution functions *P*(*r*) from SAXS data for 1mM and 10 mM FIT-27 solutions in PBS buffer (pH 7.4). Red: 1 mM, green: 10 mM. (Right) Differential *P*(*r*) showing the changes in vector length (from ~ 10 Å to ~ 35 Å, and ~45 Å) reflecting the conformational transformation of FIT-27 when the concentration changes from 1 mM to 10 mM.

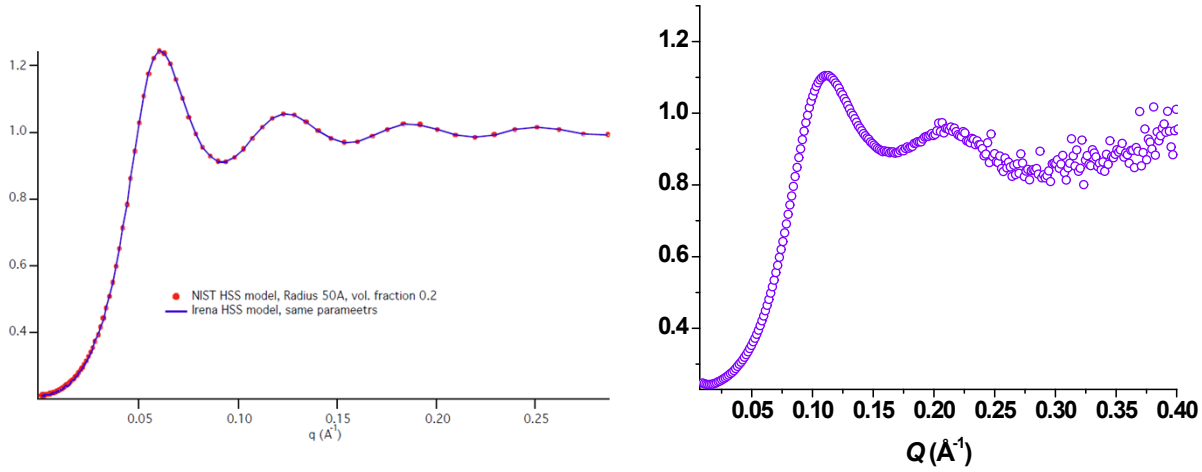

Figure S21. (Left) Hard Spheres structure factor used with *IRENA* 2.46 programs (http://www.ncnr.nist.gov/programs/sans/data/data_anal.html). (Right) Experimental structure factor $S(Q)$ observed at 100mM FIT-27 . See Figure 5(A) in the main text.

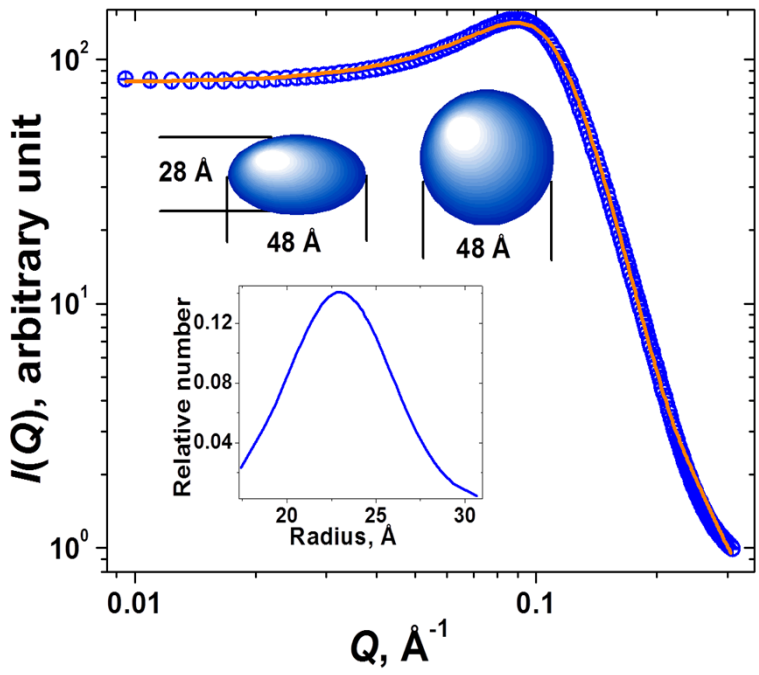

Figure S22. Size distribution modeling of 100 mM FIT-27 solution using the structure factor for hard spheres (fitting goodness, $R^2 > 0.99$). Inset shows the resulting size distribution and oblate spheroid shape of the scatterers reconstructed based on the mean radius ~ 24 Å (major semiaxis of spheroid), and the aspect ratio ~ 0.6.

Figure S22 shows the results of size distribution modeling for scattering particles and their structural organization. As seen from the inset, the scattering particles in 100 mM FIT-27 solution show rather narrow distribution of radii with the mean value ~ 24 Å. Also, the best fit of the model to experimental data ($R^2 > 0.99$) was obtained for spheroids with an aspect ratio ~ 0.6. Suggested general pictorial representation of the scatterers in 100 mM FIT-27 solution (two projections in Figure S22 shows the oblate spheroid with dimensions (thickness ~ 28 Å, diameter ~ 48 Å) very similar to those obtained for 10 mM FIT-27 solution (thickness ~ 25 Å, diameter ~ 45 Å, with an aspect ratio also ~ 0.6, see Figure 4(D) in the main text).

References

1 Z. -X. Jiang and Y. B. Yu, *J. Org. Chem.*, 2010, **75**, 2044–2049.

2 X. Yue, M. B. Taraban, L. L. Hyland and Y. B. Yu, *J. Org. Chem.,* 2012, **77**, 8879-8887.

3 J. C. Sloop, *Rep. Org. Chem.,* 2013, **3**, 1-11.

4 D. H. Wu, A. D. Chen and C. S. Johnson, *J. Magn. Reson. A,* 1995, **115**, 260-264.

5 E. O. Stejskal and J. E. Tanner, *J. Chem. Phys.,* 1965, **42**, 288-292.

6 C. J. Glinka, J. G. Barker, B. Hammouda, S. Krueger, J. J. Moyer and W. J. Orts, *J. Appl. Crystallogr.*, 1998, **31**, 430-445.

7 S. R. Kline, *J. Appl. Chrystallogr.*, 2006, **39**, 895-900.

8 D. I. Svergun, *J. Appl. Cryst.*, 1992, **25**, 495-503.

9 P. V. Konarev, V. V. Volkov, A. V. Sokolova, M. H. J. Koch and D. I. Svergun, *J Appl Cryst.*, 2003, **36**, 1277-1282.

10 D. Franke and D. I. Svergun, *J. Appl. Cryst.,* 2009, **42**, 342-346.

11 M. B. Kozin and D. I. Svergun, *J. Appl. Cryst.,* 2001*,* **34**, 33-41.

12 V. V. Volkov and D. I. Svergun, *J. Appl. Cryst.*, 2003, **36**, 860-864.

13 J. Ilavsky and P. Jemian, *J. Appl. Crystallogr.,* 2009, **42**, 347-353.

14 D. Subramanian, D. A. Ivanov, I. K. Yudin, M. A. Anisimov and J. V. Sengers, *J. Chem. Eng. Data,* 2011, **56**, 1238−1248.

15 (a) B. Chu, *Laser Light Scattering: Basic Principles and Practice*; Academic Press: Boston, 1991; (b) B. J. Berne and R. Pecora, *Dynamic Light Scattering: With Applications to Chemistry, Biology, and Physics*; Dover Publications: Mineola, NY, 2000.